Fractal Structures in Fullerene Layers: Simulation of the Growth Process

Hui Liu, Zhibin Lin, Leonid V. Zhigilei, and Petra Reinke*

Department of Materials Science and Engineering, University of Virginia, 395 McCormack Road, Charlottesville, Virginia 22904

Received: September 19, 2007; In Final Form: December 12, 2007

The molecular-level processes responsible for fractal-dendritic growth of second-layer C_{60} islands on large and compact first-layer C_{60} islands deposited on graphite substrate are investigated by a combination of scanning tunneling microscopy (STM) and kinetic Monte Carlo (kMC) simulations. Molecular dynamics (MD) simulations are performed to determine the activation barriers and jump rates for diffusion of C_{60} molecules on a C_{60} layer. The rates of the thermally activated processes, determined in MD simulations, are used in kMC simulations performed to explore the connections between the elementary growth mechanisms and the shapes of the growing islands. The geometry of the underlying substrate is found to result in the formation of two characteristic molecular arrangements along the edges of the growing islands (A-step and B-step on a close-packed surface). The difference in the molecular mobility along the A-step and B-step configurations, along with the difference in the probability of a C_{60} molecule to diffuse from a corner of an island to A-step or B-step edges of the island, are identified as key factors responsible for the formation of characteristic triangular shapes of the fractal islands and their orientation with respect to the underlying surface structure. The fractal shapes of the second-layer C_{60} islands predicted in kMC simulations are in a good agreement with STM images taken under comparable deposition conditions.

1. Introduction

Since the discovery of C_{60} in 1985, many studies have been devoted to the exploration of the unique properties of fullerenes and their derivatives[1−11] in a wide range of nanotechnology applications. The ability to control and optimize the performance of fullerene containing nanostructures relies critically on our understanding of the fullerene-substrate interactions and the mechanisms of thin film growth. The deposition of C_{60} on metal and semiconductor substrates, including Au, Ag, Ni, Cu, Si, and graphite, has been extensively studied.[6,12−18] For different substrate types and surface structures, the growing C_{60} films exhibit a wide range of interfacial bonding and electronic coupling, as well as a variety of growth modes.

The C_{60}−graphite system appears to be deceptively simple in this context, since both C_{60}−C_{60} and C_{60}−substrate interactions are of the van-der-Waals type and do not involve charge transfer across the interface. A recent scanning tunneling microscopy (STM) imaging of the growth of C_{60} layers on the graphite surface,[19] however, revealed an intriguing combination of structures where the formation of fractal-dendritic islands of C_{60} is observed on top of elliptical C_{60} islands growing directly on the graphite substrate. The formation of islands with fractal shapes has been observed in kinetically controlled growth in some metal-on-metal systems[20] and other systems[21−25] and has been described within the framework of diffusion limited aggregation (DLA) model.[26] On a qualitative level, the formation of the fractal C_{60} islands can also be described within the standard hit-and-stick DLA model with a variable atom-island sticking coefficient.[27]

In this paper, we report the results of a computational study aimed at providing a deeper quantitative understanding of the molecular-level processes responsible for the formation of fractal-dendritic C_{60} islands and elucidating the critical factors that determine the observed island shapes. The growth mechanisms of the second-layer C_{60} islands are investigated in computer simulations performed with a combination of molecular dynamic and kinetic Monte Carlo computational methods. Simulation results are compared with STM images reported in a previous publication,[19] and the relation between experimental and simulated results is discussed.

2. Experimental Setup

The experiments are performed in an Omicron Variable Temperature ultrahigh vacuum scanning probe microscope (Omicron VT UHV−SPM) system that consists of a preparation chamber and an analysis chamber containing the microscope. Atomically flat highly oriented pyrolytic graphite (HOPG) surfaces are obtained by removing top layers of a graphite sample with a scotch-tape in air, and subsequent annealing at 300 °C for at least 10 h in the UHV chamber prior to deposition. The substrate cleanliness is a prerequisite for the reproducible growth of fractal structures. The C_{60} beam is created by thermal evaporation of commercially available high-purity C_{60} powder (MerCorp) from a BN-crucible with a graphite liner. A detailed description of the experimental procedure is provided in ref 19. STM images are recorded with a sample bias voltage of 1.2 V and a tunneling current of 0.1 nA and acquired in the constant current mode at room temperature. The STM images are displayed such that the scan lines are horizontal and scanning proceeds from the bottom to the top.

3. STM Images of C_{60} Films

Figure 1 shows two representative STM images of C_{60} films deposited on HOPG at different coverages. The deposition duration is 10 s in (a), which corresponds to a coverage (total

* To whom correspondence should be addressed.

10.1021/jp0775597 CCC: $40.75
Published on Web 03/01/2008

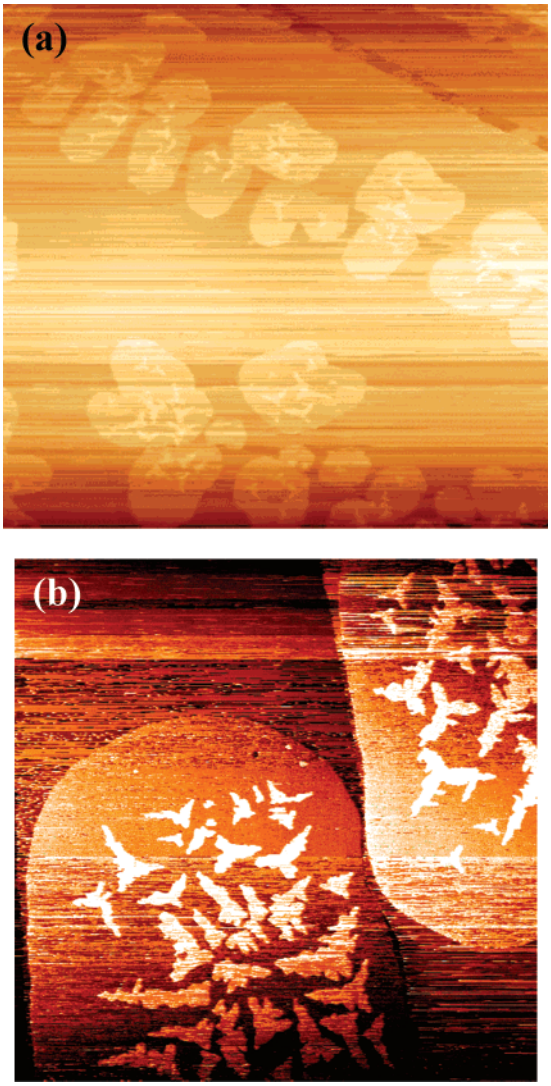

Figure 1. STM images of characteristic features of a C_{60} film growing on graphite at room temperature. In (a), the deposition duration is 10 s, the image size is 3000 × 2900 nm^2. In (b), the deposition duration is 35 s, the image size is 1500 × 1500 nm^2. The images are adapted from ref 19.

amount of fullerenes from all layers) of 0.39 monolayers (ML), as determined from the STM images. In (b) the deposition time is 35 s and the coverage amounts to 1.4 ML. The first layer of C_{60}, which is in contact with the graphite surface, grows in the form of elliptically shaped, relatively large islands. In the second layer small fractal-dendritic islands nucleate in the central parts of the underlying C_{60} islands. The straight lines intersecting the STM images from upper left to lower right corner are graphite step edges, which provide nucleation sites for the first layer islands and, at the same time, act as diffusion barriers leading to the nucleation of islands on both sides of the step. The shapes of the C_{60} islands are independent of their location with respect to the graphite steps. The STM image also shows a large number of horizontal streak-like features, which can be attributed to highly mobile C_{60} molecules moved by the STM tip due to the low adhesion of the molecules on the graphite surface.[28] The second-layer islands adopt a fractal-dendritic shape with triangular symmetry and preferred orientation in six directions, which is commensurate with the hexagonal symmetry of the underling close-packed C_{60} islands. A higher coverage of C_{60} gives rise to larger first-layer islands and a higher density of second-layer islands. It is noted that, independent of the C_{60} coverage, the second-layer islands are located in the central parts of the first-layer islands, and only a few islands form near the step edges of the first-layer islands. A detailed discussion of experimental results obtained in STM imaging of C_{60} films growing on a graphite substrate is given in ref 19.

4 Computational Method

The growth mechanisms and evolution of the shapes of the growing islands of C_{60} molecules are investigated using the kinetic Monte Carlo (kMC) computational method. This method is ideally suited for simulation of the early stages of film deposition, when the growth process is defined by a relatively small number of elementary thermally activated events defining the mobility of a C_{60} molecule. To perform a kMC simulation, we consider all possible thermally activated events that can be realized during the movement of fullerene molecules on the corrugated C_{60} surface and calculate rates for all the events. In this work, the rates of all elementary processes relevant to the growth of two-dimensional islands of C_{60} molecules on the surface of an existing close-packed fullerene island are calculated in molecular dynamics (MD) simulations. A description of the computational setups used in the MD and kMC simulations is given below.

4.1. MD Simulations of C_{60} Diffusion. The MD method is used to determine the jump rates of C_{60} molecules on a close packed fullerene surface in the presence of other C_{60} molecules, which determine the local environment of each molecule. The interaction among C_{60} molecules is described with a Girifalco potential,[29] and a potential proposed by Ruoff and Hickman[30] is used for C_{60}-graphite interactions. Both potentials adopt a simplified description of the interactions, when contributions of individual nonbonding carbon−carbon interactions are averaged to provide effective $C_{60}-C_{60}$ and C_{60}−graphite potentials. The effective potentials are defined as functions of the distance between the centers of mass of C_{60} molecules and center of mass of a molecule and the graphite plane, respectively. The cutoff distance in the interaction between C_{60} molecules is chosen to be 3.55 nm, i.e., 10 times the radius of a C_{60} molecule.[31]

The MD computational cell consists of a monolayer of C_{60} molecules arranged in a close-packed structure (10 × 10 unit cells) and placed on a graphite plane as the first layer island. The close-packed structure of the first and second C_{60} layers has been identified in high-resolution STM images presented in ref 19. A few C_{60} molecules are placed on top of the first fullerene layer in different configurations covering the range of possible local environments realized for a C_{60} molecule under the film deposition conditions. The temperature dependences of the molecular jump rates are determined by performing simulations at a range of temperatures, from 316 to 747 K. A velocity scaling is performed at the beginning of the simulation to define the desired temperature, which is then maintained in the bottom layer of C_{60} molecules during the simulation.

The rates of molecular jumps from/to all possible local configurations and diffusion events are determined by counting the number of corresponding jumps observed during an MD simulation. The jump rates are then calculated by dividing the number of jumps by the time of the simulation. The temperature dependence of a jump rate can be described by the Arrhenius-type expression

$$\nu_i = \nu_o \exp(-E_i/k_B T) \quad (1)$$

where ν_i is the jump rate for the diffusion event i, E_i is the corresponding activation energy, ν_o is the prefactor (attempt

frequency) related to the frequency of molecular vibrations and the number of possible jump directions, k_B is the Boltzmann constant, and T is the temperature. After performing simulations at different temperatures, the curve-fitting of the jump rates to eq 1 is used to determine activation energy barriers and prefactors.

The results of the MD simulations are summarized in Table 1. The schematic representation of molecular configurations used in the first column of the table is illustrated in Figure 2 for a configuration denoted as (1b). This configuration can occur in the vicinity of an existing island, as shown in Figure 2a. The hopping events occurring on the central part of the underlying fullerene island, away from the boundary of the island include the hopping of an individual C_{60} (configuration 0), as well as hopping of a C_{60} adjacent to one (configurations 1c and 1b) or two (configurations 2c−h) other second-layer molecules. The mobility of a C_{60} surrounded by 3 or more other molecules is found to be too low to contribute significantly to the development of morphology of the growing islands. These fullerene molecules are considered to be immobile. The rates of additional hopping events associated with the boundary of the first-layer island are listed in Table 1b. The values of the activation barriers and prefactors listed in Table 1 are based on simulations performed at several temperatures. For example the results from 18 different MD simulations are used to make the Arrhenius plot for configuration ($1b^{III}$), shown in Figure 3, and obtain the values of the activation barrier and the attempt frequency listed for this configuration in Table 1a.

4.2. Kinetic Monte Carlo Simulation for C_{60} Film Growth. The kMC simulations are performed on a two-dimensional (2D) lattice of binding sites that correspond to all the interstitial positions on the hexagonal close-packed structure of the first fullerene island formed on graphite. The lattice of the binding sites is created by superimposing two close-packed hexagonal 2D sub-lattices built with a lattice constant corresponding to the one of the C_{60} monolayer, 10.056 Å, and having 800×800 lattice sites each. The two hexagonal 2D sub-lattices are shifted with respect to each other by $\sqrt{3}/3 \times 10.056$ Å, so that the combined structure has all the interstitial sites of a real hexagonal close-packed surface. A round area with a radius of 250 nm, chosen to match a typical size of first-layer islands observed in STM images, is then cut from the square 2D system to generate the first-layer island used in the simulations. During the cutoff, the lattice sites connected to only one closest neighboring site are removed. The remaining lattice of 445 776 binding sites corresponds to all interstitial sites on a round 2D island composed of 222 888 C_{60} molecules.

Atomic deposition is simulated by randomly placing one C_{60} molecule on the surface. The number of simulation steps, which elapse until the next molecule is placed, are chosen to reproduce a deposition rate similar to the one used in our experiments. All of the C_{60} molecules deposited on the spherical first-layer island are allowed to jump to one of the three nearest neighboring sites, and the probabilities of the jumps are defined by the local surface configuration (see Table 1). To introduce time into kMC simulation, we use an approach based on a fixed constant time-step that keeps track of time for the entire system, e.g., refs 32 and 33. The time-step in the kMC simulations, 1.75 ns at 297 K, is chosen as the reciprocal of the total hopping rate of the C_{60} molecule that has no other molecules in the three closest neighbor shells (12 nearest binding sites), configuration (0) in Table 1. The hopping rate of an individual molecule is significantly higher than any other thermally activated event on the surface, and the probability of an individual molecule to make a jump is unity at each step. One of the three jump directions is chosen at random with equal probabilities. The probabilities of other events are determined at each time-step as the product of the time-step and the rate of the event calculated based on the values of the activation barriers and the prefactors listed in Table 1. All kMC simulations reported in this paper are performed for experimental conditions of room temperature and deposition rate of about 0.04 ML/s (one C_{60} molecule for every 68392 simulation steps).

A jump upward from graphite to a C_{60} layer has never been observed in any of the MD simulations and was therefore not included in the kMC simulations. Moreover, MD simulations indicate that there is a considerable Ehrlich-Schwoebel barrier[34] for downward jumps of second layer molecules from the first layer downward to the graphite surface (see Table 1b). A similar barrier exists for the downward jumps of third layer C_{60} deposited on top of the second layer. Consequently, the exchange of molecules between different fullerene layers is relatively rare and is, therefore, not included in the kMC simulation. The C_{60} molecules deposited on an existing fractal island are likely to form new islands, as confirmed by STM images shown in Figure 1, where the nucleation of the third layer islands on top of the second layer islands can be seen. The third layer islands exhibit the same growth behavior as the second layer islands and, at coverages considered in this work, contain small fractions of the deposited fullerene molecules. The growth of the second fullerene layer is, therefore, treated here as a process independent of the nucleation and growth of islands in the third layer, and the molecules deposited on top of the second layer are not included in the kMC simulations.

5. Simulation Results and Discussion

The growth of the second-layer C_{60} islands in a kMC simulation of room-temperature deposition with the rate of 0.04 ML/s is illustrated in Figure 4. The round boundaries of the first-layer islands are depicted by circles. At the early stage of the deposition, after several molecules are deposited, two molecules can occasionally meet and form a dimer, the lifetime of which is approximately 2.75 ns, as can be estimated from the values of the activation energies and the prefactors listed for the configuration (1b) in Table 1. During the lifetime of a dimer, if another molecule attaches to it, a cluster of three molecules forms and becomes a nucleation center. The lifetime of a cluster of three C_{60} molecules arranged in the configuration (2c) is approximately 2824 ns at room temperature, while the lifetime is much longer if the molecules are arranged in configuration (2d).

The stable initial clusters grow in the course of the deposition and develop into relatively compact islands of a characteristic triangular star shape with three major branches, e.g., Figure 4 at 0.02 and 0.05 ML. As the coverage increases, the island shape gradually becomes more dendritic and finally becomes ramified. Six preferred growth orientation directions can be identified at low coverages, which agree with the shapes observed in STM images shown in Figure 1. Because of the growth competition among different islands, the growth of some of the branches becomes obstructed and the islands start to merge at coverages exceeding ~0.3 ML.

There is a clear tendency of the second-layer islands to avoid nucleation close to the edge of the first-layer island, which also agrees with experimental observations, Figure 1a. The coverage of the first layer by the second layer in the STM image shown in Figure 1a is 0.09, the same as in the snapshot from kMC simulation in Figure 4c. A visual analysis of Figure 1a and 4c

TABLE 1: (a) Energy Barriers, Attempt Frequencies, and Probabilities of Diffusion Jump Events on a Fullerene Island[a]

Terrace	Jump to I Energy barrier (meV) Attempt frequency ($\times 10^{12}$ s^{-1})	Jump to II Energy barrier (meV) Attempt frequency ($\times 10^{12}$ s^{-1})	Jump to III Energy barrier (meV) Attempt frequency ($\times 10^{12}$ s^{-1})
0 (without neighbors - basic movement)	$E_0 = 178 \pm 4$ $\nu_0 = 0.2 \pm 0.03$	$E_0 = 178 \pm 4$ $\nu_0 = 0.2 \pm 0.03$	$E_0 = 178 \pm 4$ $\nu_0 = 0.2 \pm 0.03$
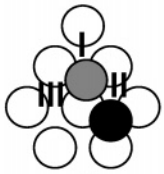 **1b**	$E_{1b}^{I} = 429 \pm 57$ $\nu_{1b}^{I} = 0.65 \pm 0.09$	$E_{1b}^{II} = \infty$ †	$E_{1b}^{III} = 185 \pm 6$ $\nu_{1b}^{III} = 0.25 \pm 0.04$
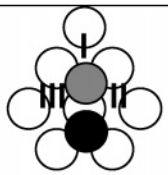 **1c**	$P_{1c}^{I} = 50\%$ *	$P_{1c}^{II} = 50\%$ *	$P_{1c}^{III} = 0\%$ *
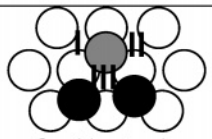 **2c (A-step)**	$E_{2c}^{I} = 354 \pm 63$ $\nu_{2c}^{I} = 0.06 \pm 0.01$	$E_{2c}^{II} = 354 \pm 63$ $\nu_{2c}^{II} = 0.06 \pm 0.01$	$E_{2c}^{III} = \infty$ †
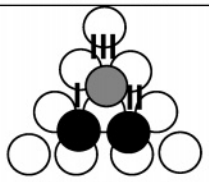 **2d (B-step)**	$E_{2d}^{I} = \infty$ †	$E_{2d}^{II} = \infty$ †	$E_{2d}^{III} = \infty$ †
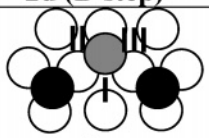 **2e**	$P_{2e}^{I} = 98.24 \pm 0.3\%$*	$P_{2e}^{II} = 0.88 \pm 0.15\%$*	$P_{2e}^{III} = 0.88 \pm 0.15\%$*
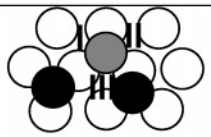 **2f**	$E_{2f}^{I} = \infty$ †	$E_{2f}^{II} = \infty$ †	$E_{2f}^{III} = \infty$ †
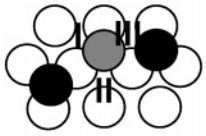 **2g**	$P_{2g}^{I} = 99.86 \pm 0.1\%$*	$P_{2g}^{II} = 0.14 \pm 0.1\%$*	$P_{2g}^{III} = 0\%$
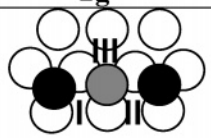 **2h**	$E_{2h}^{I} = \infty$ †	$E_{2h}^{II} = \infty$ †	$E_{2h}^{III} = \infty$ †
3 (three or more neighbors)	$E_3 = \infty$ †	$E_3 = \infty$ †	$E_3 = \infty$ †

TABLE 1: (b)

Boundary	Jump to I	Jump to II	Jump to III
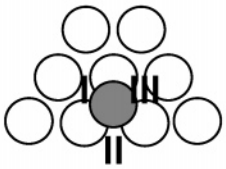 **j**	$P_j^{I} = 45. \pm 1\ \%^{*}$	$P_j^{II} = 10.0 \pm 0.5\ \%^{*}$	$P_j^{III} = 45. \pm 1\ \%^{*}$
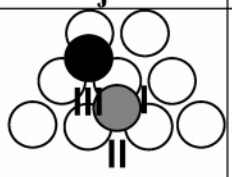 **ja**	$P_{ja}^{I} = 99.97 \pm 0.03\ \%^{*}$	$P_{ja}^{II} = 0.03 \pm 0.03\ \%^{*}$	$P_{ja}^{III} = 0\%$
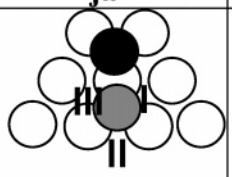 **jb**	$P_{jb}^{I} = 50\ \%^{*}$	$P_{jb}^{II} = 0\ \%$	$P_{jb}^{III} = 50\ \%$
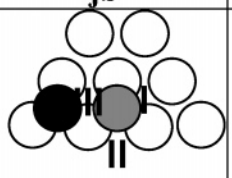 **jc**	$E_{jc}^{I} = 207 \pm 4$ $\nu_{jc}^{I} = 0.29 \pm 0.01$	$E_{jc}^{II} = 354 \pm 53$ $\nu_{jc}^{II} = 0.3 \pm 0.05$	$E_{jc}^{III} = \infty\ ^{\dagger}$
j2 (two or more neighbors)	$E_{j2} = \infty\ ^{\dagger}$	$E_{j2} = \infty\ ^{\dagger}$	$E_{j2} = \infty\ ^{\dagger}$

[a] The values for the energy barriers and attempt frequencies are obtained from MD simulations as described in the text. The starting configurations are schematically shown in the first column: the hollow circles represent C_{60} molecules that form a close-packed structure of the first-layer island, gray and black circles represent C_{60} molecules deposited on the first-layer island. The molecules shown by black circles are immobilized by the presence of other molecules (as an example, immobile molecules in configuration 1b are shown in Figure 2a), whereas the jumps of the molecules shown by gray circles are recorded in the MD simulations. The three possible hopping destinations are marked for each mobile C_{60} molecule as I, II, and III, with corresponding energy barriers, attempt frequencies, and relative jump probabilities shown in columns 2, 3, and 4, respectively. In the nomenclature used to label the jumps, the superscript denotes the hopping destination and the subscript denotes the initial configuration as illustrated in the first column. Table 1a lists information for all movements occurring on the fullerene island, except for the ones near the edge of the island. Table 1b characterizes the possible jumps of a fullerene molecule positioned close to the boundary of a first-layer island (the bottom row of 5 fullerene molecules in the schematic drawings are at the edge of the island in this case). The * denotes that the initial configuration is a metastable state. The jump rate is higher than that of the basic movement. Only the relative probabilities (P) of jumping to the three directions are recorded. The † denotes that the initial configuration is a stable state. The number of jumps at 700 K (<10 jumps per 20 ns) is insufficient to determine the activation energy and the jump frequency at room temperature.

indicates that the shapes of the islands observed in the simulation and experiment are similar. In order to perform a quantitative comparison between the experimental results and the predictions of the kMC simulation, the fractal dimension of the second-layer islands is calculated for different times during the simulation, Figure 5. To ensure the direct connection with experimental results, the same box-counting method,[35] previously used in analysis of the STM images,[19] is used to characterize the shapes of the simulated islands. In this method, the simulated images, shown in Figure 4, are transformed to a black-and-white mode, and then scanned by Scion image analysis software. To obtain the fractal dimension, an image of the second-layer islands is divided into squares with various sizes (A) and the occupied (black) squares are counted. The occupation number N scales as $\ln N \propto D \ln A$, where D is the fractal dimension. The configurations on a surface may have a fractal dimension between 1 and 2, where a fractal dimension of 1 corresponds to a linear arrangement of molecules and a fractal dimension of 2 corresponds to a round island. In the simulation, the fractal dimension of the islands increases from 1.5 to 1.9 during the deposition, with changes in the rate of the increase reflecting the changes in the growth mechanisms. At the onset of the growth (coverage less than ~15%), the fractal dimension increases rapidly as the individual small islands transition from their initial triangular star shapes to characteristic dendritic shapes with multiple branches, Figure 4. At these coverages, the islands are separated from each other and the growth process of individual islands is largely unaffected by the presence of other islands. At higher coverages, the growth competition among islands, coalescence of islands, and the limitation of the size of the first-layer island lead to

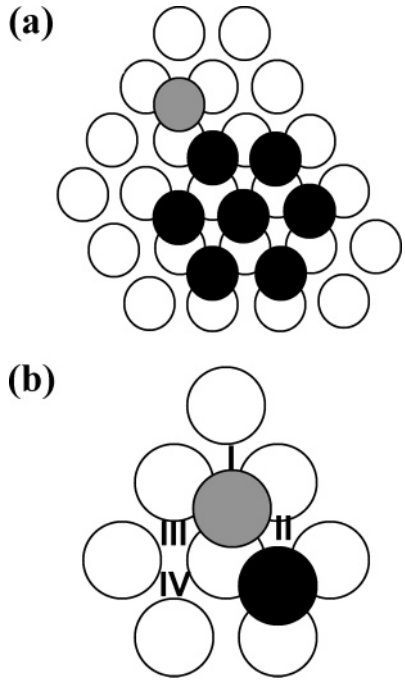

Figure 2. Example of a molecular configuration used in MD simulations (a) and a corresponding schematic representation used in the first column of Table 1 (b). The molecules shown by black circles are immobilized by the presence of the surrounding molecules. The molecule shown by the gray circle can move during an MD simulation and the jump frequencies are calculated for different temperatures and different jump destinations to provide the data listed in Table 1. The configuration illustrated here corresponds for configuration (1b) in Table 1.

the increase of the compactness of the growing islands which, in turn, is reflected in the further increase of the fractal dimension.

The fractal dimensions of the second-layer islands predicted in the kMC simulation can be related to the ones calculated for STM images and shown in Figure 5 for comparison. The coverage indicated in the graph is the coverage of the first layer island with second layer islands. For the simulation this value is precisely known, but for the experimental data an error of about 10% in determination of the coverage values from the STM images is included in the graphs shown in Figure 5. The error bars for the values of the fractal dimension result from the application of the box-counting method. The agreement between the simulation and experiment is good for moderate coverages of up to ~0.3 ML, albeit the increase in the fractal dimension is somewhat steeper in the simulation. The disagreement is more pronounced at larger coverages, where some of the assumptions made in the computational model, such as the ones of the negligible contribution from molecules deposited on top of the growing islands and the constant size of the first-layer island during the growth process, begin to break down.

The diffusion limited aggregation (DLA) model, which assumes that particles undergo random walk and stick to the surface of a growing aggregate whenever they encounter it, has been used extensively to explain the formation of fractal structures. The fractal dimension for 2D fractal-dendritic islands formed by the conventional DLA (with a sticking coefficient of one) is 1.67, independent of the coverage. Wynblatt et al.[36] developed a modified DLA model, which allowed for site-specific sticking coefficients different from unity. The modified DLA successfully explained the width of the growing branches in dendrite-like gold islands and yielded the fractal dimensions of 1.7~1.9.[36] This model, however, fails to account for the appearance of the triangular shape and preferential orientation of the islands, which requires a more detailed consideration of the molecule−surface interactions and the elementary molecular-level processes responsible for the growth of the islands.

To explore which energy barriers have the most prominent effect on the appearance of the triangular star shape, we artificially changed the rates of different diffusion events and performed kMC simulations for these modified conditions. It is found that the energy barriers related to the diffusion along A-step (configuration (2c) in Table 1) and B-step (configuration (2d) in Table 1) of a growing island have the most prominent impact on the shapes of the islands. Figure 6 illustrates the shapes of the islands obtained in simulations performed with various values of E_{2c}^{I} and E_{2c}^{II} while all other parameters remained unchanged. Because of the symmetry of the configuration, E_{2c}^{I} and E_{2c}^{II} have the same value. The snapshots in Figure 6 are shown for the same number simulation steps of 3×10^9 performed with the same deposition rate of 0.04 ML/s, which then corresponds to a final first layer coverage of 0.09−0.11 ML. At $E_{2c}^{I,II} = 100$ meV, the island has a compact and irregular shape, Figure 6a. As the value of E_{2c}^{I} increases, the islands gradually develop branched triangular or triangular star shapes, Figure 6, panels c and d, and, at the highest values of $E_{2c}^{I,II}$, adopt triangular shapes with fragmented edges, Figure 6, panels e and f. Compared to the experimental results, the island shapes in Figure 6d exhibit a close similarity to the second-layer C_{60} islands in STM image, confirming that the value of the energy barrier found in MD simulations is close to the experimental one.

The results of the simulations performed for different ratios of the jump rates to site III and site I in the configuration (1b), with the overall probability of a diffusion event associated with this configuration unchanged, is illustrated in Figure 7. If the ratio E_{1b}^{III}/E_{1b}^{I} is adjusted so that relatively more jumps to the neighbor sites I occur (small ratio of probabilities P_{1b}^{III}/P_{1b}^{I}), the islands are large and compact, Figure 7a. As the ratio increases, the islands become smaller and more numerous, with the triangular star shape becoming more pronounced. The island density is related to the ratio of P_{1b}^{III}/P_{1b}^{I}, since more islands form if the possibility of the detachment of a molecule from an island is higher.

The energy barriers, which are related to the jump events close to the boundary of the first layer, affect only the island density if the deposition rate is constant. In particular, the number of the second-layer islands obtained in kMC simulations performed with various values of P_j^{II}, keeping all other rates unchanged, is shown in Figure 8 for the area of the simulated first-layer island of 1.96×10^5 nm^2. The simulations are performed for 3×10^9 simulation steps with the same deposition rate of 0.04 ML/s. The value of P_j^{II} reflects the magnitude of the Ehrlich-Schwoebel barrier[34] at step edges. The number of islands is at its maximum value when $P_j^{II} = 0\%$, which means that no molecules at the step edge can jump downward. As P_j^{II} increases, the number of islands decreases first and then saturates at a constant value of about 6 at $P_j^{II} > 5\%$. It is apparent from the insets in Figure 8 that the simulated second-layer islands preserve the triangular star shape independent of the value of P_j^{II}. The value of $P_j^{II} = 10\%$ was obtained from MD simulations and used in the kMC simulation. The average number of islands on a 1.96×10^5 nm^2 first-layer island in the experiment is 4.1. The discrepancy between the simulations and experiments can be related to the assumption of the fixed boundary of the first layer island in the kMC simulation.

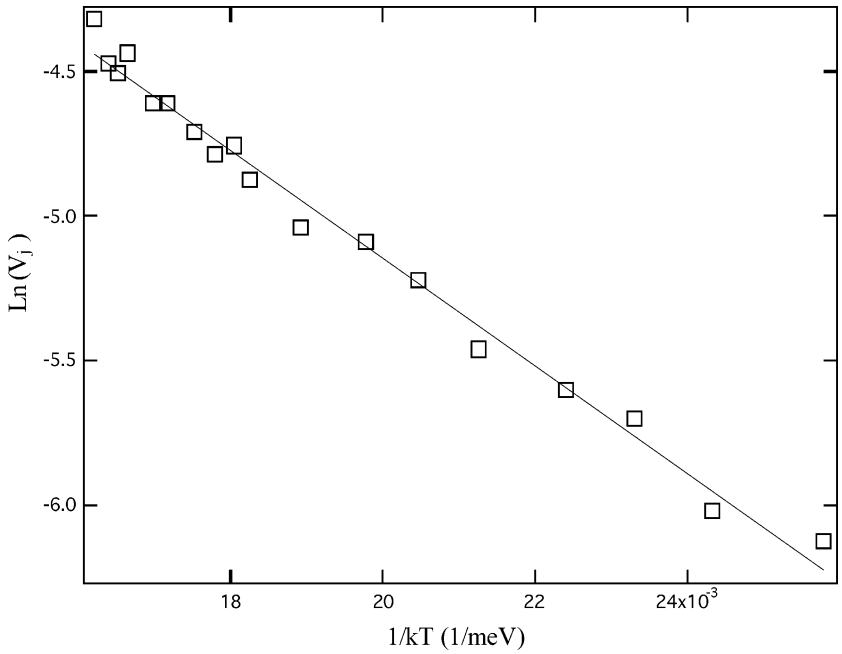

Figure 3. Example of Arrhenius plots used to determine the activation barriers and prefactors in eq 1. The results are shown for configuration (1b) in Table 1a. The calculation of the jump rate is based on 262 jump events recorded at the highest temperature and 43 jumps recorded at the lowest temperature used in this series of MD simulations.

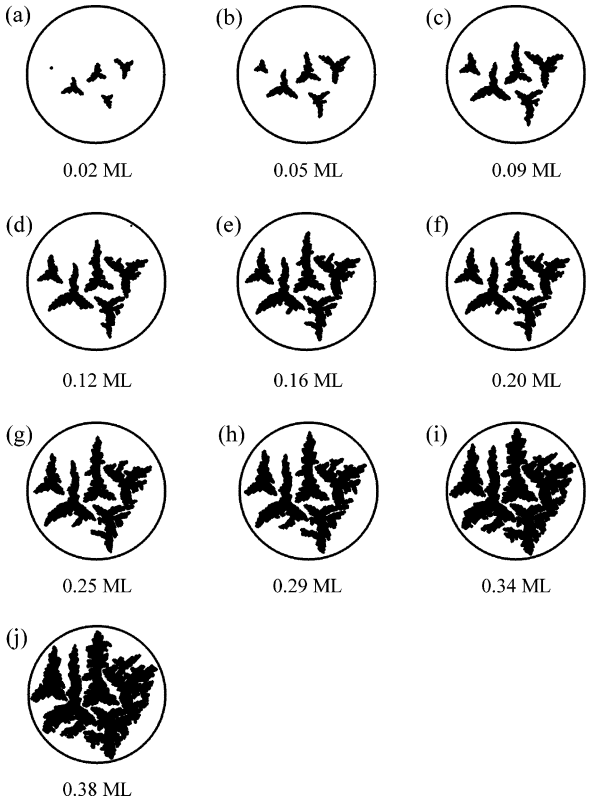

Figure 4. Sequential growth progression of the second-layer C_{60} islands predicted in a kMC simulation. The coverages are 0.02, 0.05, 0.09, 0.12, 0.16, 0.25, 0.29, 0.34, and 0.38 ML, respectively. The round boundary of the first-layer C_{60} island is shown by circles.

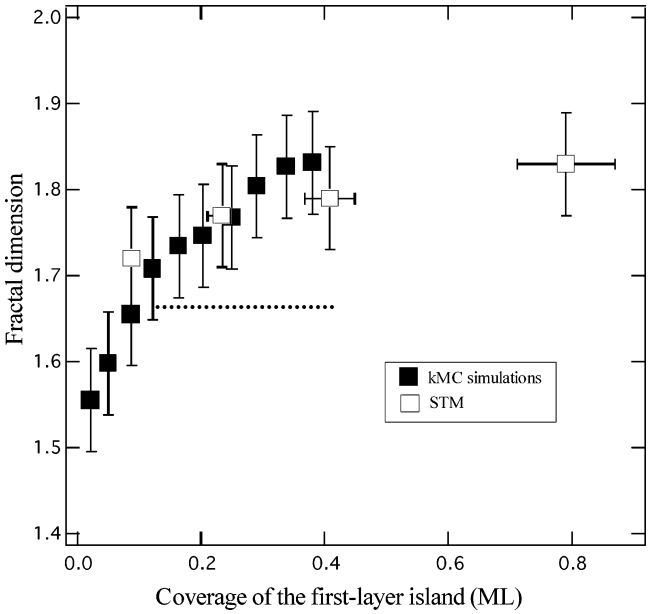

Figure 5. Fractal dimension of the second-layer islands as a function of coverage predicted in the kMC simulation and calculated from STM images (Figure 1, panels a and b, in ref 19). The fractal dimension of islands predicted by DLA model is 1.67 and is shown by the horizontal dashed line.

The triangular star shape of the second-layer islands is the prominent feature of the growth of C_{60} on graphite, Figure 1. However, both the conventional DLA model and Wynblatt's model[30] fail to predict the triangular shape of the second-layer C_{60} islands. These models do not distinguish the A-step and B-step geometries, which are inherent to the islands growing on hexagonal close packed surfaces. For metal-on-metal systems,[20,37,38] it is well-known that activation energy barriers for atomic diffusion along a A-step are different from those along a B-step, which strongly affects the shapes of the growing islands. For example, Pt growth on Pt(111) exhibits ramified islands at 300 K and compact islands of triangular shape at 400 K[20]. The kinetic Monte Carlo simulations distinguish between the atomic mobility along A- and B-steps and, as a result, successfully reproduce the fractal-dendritic shapes of the second-layer C_{60} islands.

The orientation of the dendritic islands with respect to the underlying close-packed first-layer fullerene lattice stems from anisotropy of the C_{60} diffusion along the edges of the growing islands. It is found in the kMC simulations discussed above

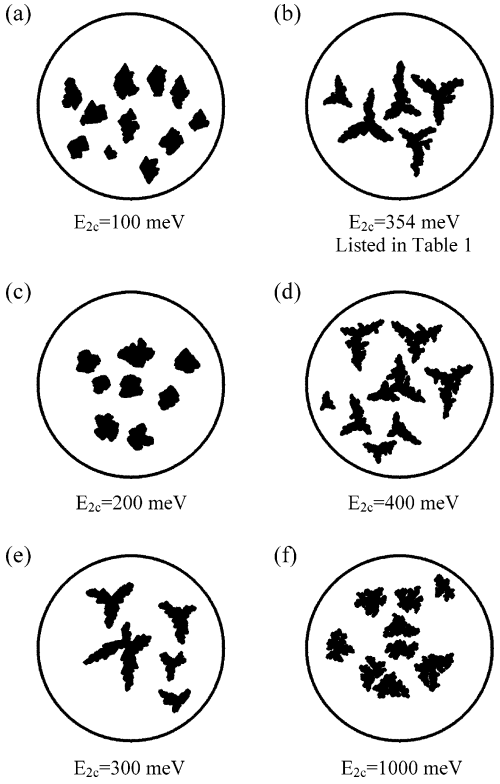

Figure 6. Second-layer islands obtained in simulations performed with various values of E_{2c}^{I} (E_{2c}^{II}) and other parameters unchanged. The simulation is performed for 3×10^9 steps with a deposition rate of 0.04 ML/s.

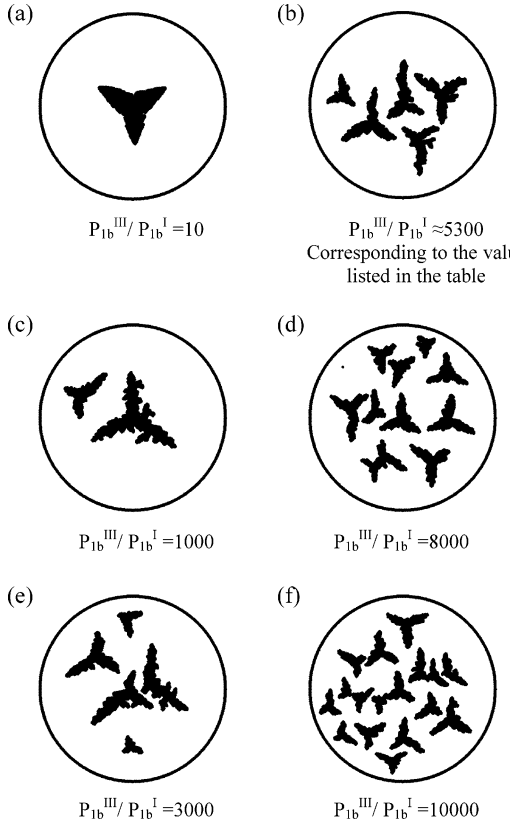

Figure 7. Second-layer islands obtained in simulations performed with different ratios of the jump rates to the neighbor site III and the neighbor site I, while keep the overall probability of all jump events in configuration (1b) unchanged. The simulation is performed for 3×10^9 steps with a deposition rate of 0.04 ML/s.

that the ratio of E_{1b}^{III}/E_{1b}^{I}, characterizing the relative probabilities of a corner atom to hop to either an A-step or a B-step, and the value of E_{2c}^{I} (E_{2c}^{II}), which characterizes the diffusion along an A-step, are the most important parameters determining the shapes of the second-layer islands. From the configuration shown in Figure 2, a molecule located at a corner of an island can hop to one of the two neighboring sites adjacent to the island, I and III. If followed by a hop to a neighboring site IV, the hop to the neighbor site III can move a mobile C_{60} to the A-step. Direct diffusion to the B-step is less likely since a hop to site II has an extremely high local activation barrier and an alternative pass involves a sequence of several hops. Therefore, diffusion to A-steps is much more preferable for a corner molecule than diffusion to B-steps. The results of MD simulations suggest that the edge diffusion along a B-step (E_{2d}^{I}, E_{2d}^{II}) is a very slow process, which makes the diffusion barrier along an A-step (E_{2c}^{I}, E_{2c}^{II}) a critical factor in the defining the shapes of the growing islands. The mobility of a molecule along an A-step can be characterized by a diffusion coefficient defined as $D = \nu a^2/z$, where ν is the frequency of hops along the A-step, a is the jump distance, and z is 2 for the one-dimensional diffusion. Using the values of the energy barrier and attempt frequency listed in Table 1, the room-temperature diffusion coefficients along A-steps can be calculated to be 3×10^{-14} m^2/s. A smaller values of E_{2c}^{I} (E_{2c}^{II}) can destroy the 3-fold symmetry in the islands since the fast diffusion along A-step would counteract the anisotropy that originate in the large ratio of P_{1b}^{III}/P_{1b}^{I}. If E_{2c}^{I} (E_{2c}^{II}) is too large, however, the mobility along the edges would be small and random attachments to island edges would results in islands with fragmented edges instead of the triangular star shapes observed in STM images.

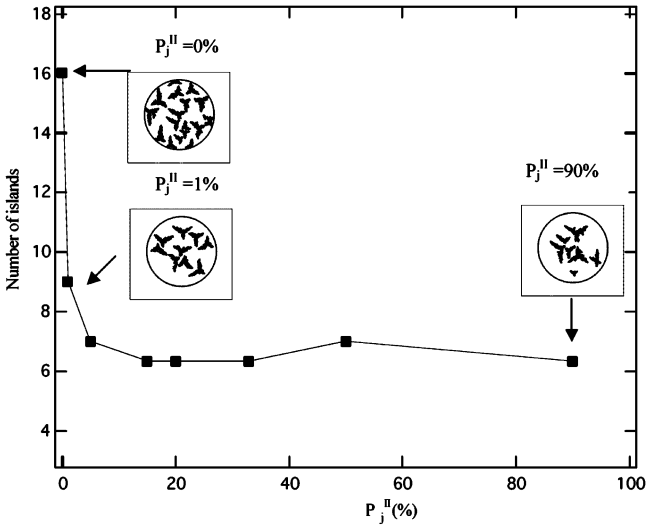

Figure 8. Number of the second-layer islands predicted in kMC simulations with various values of P_j^{II}. The area of the first-layer islands is 1.96×10^5 nm^2. The simulations are performed for 3×10^9 steps with a deposition rate of 0.04 ML/s. Each point in the plot is calculated based on the results of 3 simulations. Insets show examples of molecular configurations for three values of P_j^{II}.

6. Conclusion

The results of kMC simulations provide a detailed molecular-level picture of fractal-dendritic growth of second-layer C_{60} islands on compact first-layer C_{60} islands deposited on graphite substrate. The simulations are parametrized based on MD

simulations performed at different temperatures and used to determine the rates of all relevant thermally activated processes responsible for the island nucleation and growth during the deposition. The geometry of the underlying substrate is found to result in the formation of two characteristic molecular arrangements along the edges of the growing islands (A-step and B-step on a close-packed surface). The difference in the molecular ability along the A-step and B-step configurations, along with the difference in the probability of a C_{60} molecule to diffuse from a corner of an island to A-step or B-step edges of the island, are identified as key factors responsible for the formation of characteristic triangular shapes of the fractal islands and their orientation with respect to the underlying surface structure. The fractal shapes of the second-layer C_{60} islands predicted in kMC simulations are in a good agreement with STM images taken under comparable deposition conditions. A further refinement of the model aimed at improvement of the quantitative agreement between simulation and experiment would incorporate a description of the molecular exchange between layers and the growth of the first layer island during the deposition.

Acknowledgment. This work was supported by the MRSEC Center for Nanoscopic Materials Design sponsored by the National Science Foundation and the start-up funding from the University of Virginia (P.R.).

References and Notes

(1) Robinson, A. P. G.; Palmer, R. E.; Tada, T.; Kanayama, T.; Preece, J. A. *Appl. Phys. Lett.* **1998**, *72*, 1302.
(2) Shinohara, H. *Rep. Prog. Phys.* **2000**, *63*, 843.
(3) Forro, L.; Mihaly, L. *Rep. Prog. Phys.* **2001**, *64*, 649 .
(4) Haddon, R. C.; Perel, A. S.; Morris, R. C.; Palstra, T. T. M.; Hebard, A. F.; Fleming, R. M. *Appl. Phys. Lett.* **1995**, *67*, 121.
(5) Sun, Y. P.; Riggs, J. E. *Int. Rev. Phys. Chem.* **1999**, *18*, 43.
(6) Joachim, C.; Gimzewski, J. K.; Schlittler, R. R.; Chavy, C. *Phys. Rev. Lett.* **1995**, *74*, 2102.
(7) Dresselhaus, M. S.; Dresselhaus, G.; Eklund, P. C. *Science of Fullerenes and Carbon Nanotubes*; Academic Press: San Diego, CA, 1996.
(8) Gunnarsson, O. *Rev. Mod. Phys.* **1997**, *69*, 575.
(9) Rudolf, P.; Golden, M. S.; Bruhwiler, P. A. *J. Electron. Spectr. Rel. Phen.* **1999**, *100*, 409.
(10) Fisher, A.; Osawa, E. *Perspectives of Fullerene Nanotechnology*; Kluwer Academic Publishers: Dordrecht, Netherlands, 2002.
(11) Licht, S.; Khaselev, O.; Ramakrishnan, P. A.; Faiman, D.; Katz, E. A.; Shames, A.; Goren, S. *Solar Energy Mater. Solar Cells* **1998**, *51*, 9.
(12) Gimzewski, J. K.; Modesti, S.; Schlittler, R. R. *Phys. Rev. Lett.* **1994**, *72*, 1036.
(13) Rafii-Tabar, H.;Ghafoori-tabrizi, K. *Prog. Surf. Sci.* **2001**, *67*, 217.
(14) Girard, C. *Phys. Rev. B* **1994**, *49*, 11425.
(15) Rey, C.; Garcia-Rodeja; J.; Gallego, L. J. *Phys. Rev. B* **1997**, *55*, 7190.
(16) Gravil, P. A.; Devel, M.; Lambin, P.; Bouju, X.; Girard, C.; Lucas, A. A. *Phys. Rev. B* **1996**, *53*, 1622.
(17) Rafii-Tabar, H.; Jurczyszyn, L.; Stankiewicz, B. *J. Phys. Condens. Matter.* **2000**, *12*, 5551.
(18) Girifalco, L. A.; Hodak, M.;Lee, R. S. *Phys. Rev. B* **2000**, *62*, 13104.
(19) Liu, H.; Reinke, P. *J. Chem. Phys.* **2006**, *124*, 164707.
(20) Hohage, M.; Bott, M.; Morgenstern, M.; Zhang, Z.; Michely, T.; Comsa, G. *Phys. Rev. Lett.* **1996**, *76*, 2366.
(21) Meyer zu Heringdorf, F. J.; Reuter, M. C.; Tromp, R. M. *Appl. Phys. A* **2004**, *78*, 787.
(22) Chen, W.; Chen, S.; Zhang, H. L.; Xu, H.; Qi, D. C.; Gao, X. Y.; Loh, K. P.; Wee, A. T. S. *Surf. Sci.* **2007**, *601*, 2994.
(23) Lee, C. M.; Yang, S.-H.; Mun, B.-J.; Ross, P. N., Jr. *Surf. Sci.* **2001**, *477*, 126.
(24) Chen, H. L. Z. W.; Xu, H.; Tok, E. S.; Loh, K. P.; Wee, A. T. S. *J. Phys. Chem. B* **2006**, *110*, 21873.
(25) Muller, M.; Michely, T. *Phys. Rev. B* **2005**, *71*, 075407.
(26) Witten, T. A.; Sander, L. M. *Phys. Rev. Lett.* **1981**, *47*, 1400.
(27) Zhang, Z.; Chen, X.; Lagally, M. G. *Phys. Rev. Lett.* **1994**, *73*, 1829.
(28) Bartels, L.; Meyer, G.; Rider, K. H. *Phys. Rev. Lett.* **1997**, *79*, 697.
(29) Girifalco, L. A. *J. Phys. Chem.* **1992**, *96*, 858.
(30) Ruoff, R. S.; Hichman, A. P. *J. Phys. Chem.* **1993**, *97*, 2494.
(31) Hodak, M.; Girifalco, L. A. *Phys. Rev. B* **2003**, *68*, 085405.
(32) Srivastava, D.; Garrison, B. J. *J. Chem. Phys.* **1991**, *95*, 6885.
(33) Dawnkaski, E. J.; Srivastava, D.; Garrison, B. J. *J. Chem. Phys.* **1995**, *102*, 9401.
(34) Schwoebel, R. L.; Shipsey, E. J. *J. Appl. Phys.* **1966**, *37*, 3682.
(35) Niemeyer, L.; Pietronero, L.; Wiesmann, H. J. *Phys. Rev. Lett.* **1986**, *52*, 1033.
(36) Wynblatt, P.; Metosi, J. J.; Heyraud, J. C. *J. Cryst. Growth* **1990**, *102*, 618.
(37) Liu, S.; Zhang, Z.; Comsa, G.; Metiu, H. *Phys. Rev. Lett.* **1993**, *71*, 2967.
(38) Jacobsen, J.; Jacobsen, K. W.; Stoltze, P.; Norskov, J. K. *Phys. Rev. Lett.* **1995**, *74*, 2295.